Critical Behavior in a Binary Polymer Blend as Studied by Static and Dynamic Light Scattering

ARTICLE *in* THE JOURNAL OF CHEMICAL PHYSICS · OCTOBER 1992

Impact Factor: 2.95 · DOI: 10.1063/1.463748

3 AUTHORS, INCLUDING:

Gerhard Meier
Forschungszentrum Jülich
111 PUBLICATIONS **2,252** CITATIONS

Critical behavior in a binary polymer blend as studied by static and dynamic light scattering

G. Meier, B. Momper, and E. W. Fischer

Citation: J. Chem. Phys. **97**, 5884 (1992); doi: 10.1063/1.463748
View online: http://dx.doi.org/10.1063/1.463748
View Table of Contents: http://jcp.aip.org/resource/1/JCPSA6/v97/i8
Published by the American Institute of Physics.

Critical behavior in a binary polymer blend as studied by static and dynamic light scattering

G. Meier, B. Momper, and E. W. Fischer
Max Planck Institut für Polymerforschung, Postfach 3148, W 6500 Mainz, Germany

(Received 23 January 1992; accepted 29 June 1992)

We report static and dynamic light scattering experiments of an almost symmetric polymer mixture made up from poly(dimethylsiloxane) (PDMS), $N=260$, and poly(ethylmethylsiloxane) (PEMS), $N=340$, with N being the degree of polymerization, both below the entanglement molecular weights. The mixture exhibits an upper critical solution temperature $T_c \simeq 57\,^{\circ}\mathrm{C}$. The measurements were performed at the critical composition $\phi_{c,\mathrm{PEMS}} = 0.465$ in a broad temperature range in the one phase region above the spinodal point. The main results for the static case are: the temperature dependence of the static structure factor $S(q=0)$ can be described by a mean field behavior. For T close to T_c, a crossover to an Ising behavior is observed according to a modified Ginzburg criterion. From the angular dependence of $S(q)$, the static correlation length ξ is determined via an Ornstein–Zernike plot. Our experimentally determined values for $\lim_{T\to\infty} S(0)$ and $\lim_{T\to\infty} \xi$, respectively, are in agreement with theoretical predictions. For the dynamic case, the main results are summarized as follows: as expected, the mutual diffusion coefficient $\tilde{D}$, accessible by quasielastic light scattering, shows a critical slowing down for $T\to T_c$. For $q\xi \gg 1$, we observe that the q scaling of the Rayleigh linewidth Γ changes from a q^2 to a q^3 behavior, which is in agreement with mode coupled expressions. This occurs in a relatively broad temperature range, due mainly to the fact that polymer mixtures exhibit a larger $\xi_0 \propto \sqrt{N}$, on the contrary to any other systems known, which allows us therefore to reach the region $q\xi \gg 1$ even with light scattering easily. From the separation of the measured Rayleigh linewidth into a critical part and a background part, we have estimated the crossover between mode coupled to nonmode coupled dynamics. It is governed by the coil size. The scaling predictions for the critical part and the background part of the linewidth are in agreement with the predictions of the mode coupled theory by Kawasaki and subsequently by Fredrickson. We find that the mode coupled dynamics reaches far into the mean field regime which is not yet understood by theory. Furthermore, we can show that the critical part of the linewidth data is well represented by the Kawasaki shape function including the viscosity correction. Finally, we have estimated a segmental mobility $W^0 \propto \tilde{D}\cdot S(q=0)$ which can be interpreted being a segmental quantity only down to characteristic lengths $\xi(T) \simeq R_g$. For ξ larger than the coil dimensions, $W^0 \propto \xi$ as predicted by mode coupled dynamics.

I. INTRODUCTION

The static equilibrium properties of binary polymer mixtures have been investigated by different scattering methods like time averaged light scattering,[1–3] small angle x-ray scattering (SAXS),[4,5] and mainly small angle neutron scattering (SANS).[6–12] As a main result, it was found that the scattering pattern can be described adequately by using the mean field approximation.[13] However, close to the critical point of phase separation, the static properties may exhibit Ising-like behavior, which has been reported by SANS for few systems so far.[7,14] This crossover from mean field to Ising depends in a specific way on the degree of polymerization which can be estimated from the Ginzburg criterion.[15,16] Although, concerning this point only few data have been published, the agreement between experiment and theory is poor. We intend therefore to compare our data with a theoretical prediction which has been published recently by Bates *et al.*[17,18]

The dynamic critical behavior of polymer blends, on the other hand, is experimentally largely unexplored. The use of x-ray and neutron real time experiments is very limited due to poor time resolution, and naturally the use of dynamic light scattering becomes advantageous. In the past, it was mostly employed to study static and dynamic properties of simple liquid mixtures[19] or polymers in solution.[20,21] Those results are discussed within the mode coupling theory[22–24] and the dynamical renormalization group theory.[25,26] In a new extended paper by Stepanek *et al.*,[18] the first analysis of dynamic light scattering data of critical fluctuations in a binary polymer mixture in terms of mode coupled expressions has been presented based on the theoretical work of Fredrickson.[27,28] The authors could localize the crossover between mean field and nonmean field behavior and used the dynamic light scattering to reveal the fact that mode coupled critical dynamic is valid far into the mean field regime. We additionally report here, furthermore, a comparison with the Kawasaki shape function including the evaluation of the background and an analysis

 0021-9606/92/205884-14$006.00

of the range of applicability of the concept of a microscopic Onsager coefficient to relate the static susceptibility with microscopic properties in the framework of the Rouse theory.[29]

II. THEORETICAL BACKGROUND

A. Static properties

Using the random phase approximation,[13,30,31] we can write down the expression for the static structure factor $S(q)$ of a polymer mixture

$$\frac{1}{S(q)}=\frac{1}{S^{\text{n.i.}}(q)}-V(q), \tag{1}$$

where n.i. means noninteracting and $V(q)$ is the Fourier transform of the interactions. They are assumed to be of short range, in the order of a segment length. Using now a classical mean field argument, namely the Flory–Huggins lattice model, we can evaluate the structure factor for the noninteracting case to be (for two components)

$$\frac{1}{S^{\text{n.i.}}(q)}=\frac{1}{\phi_A S_A(q)}+\frac{1}{\phi_B S_B(q)}. \tag{2}$$

There $S_A(q)$ and $S_B(q)$ are the scattering functions of the individual chains. If we assume them to obey Gauss statistics having N_A and N_B segments of size σ_A and σ_B, then the single chain scattering functions are given by

$$S_i(q)=N_i f_D(\tfrac{1}{6}N_i\sigma_i^2 q^2), \tag{3}$$

where $f_D(x)$ is the Debye function

$$f_D(x)=\frac{2}{x}\left[1-\left(\frac{1-e^{-x}}{x}\right)\right]. \tag{4}$$

For wave vectors relevant to light scattering q's (the relevant range with $\lambda=514.5$ nm is $9\times10^{-4}<q<3.5\times10^{-3}$ Å^{-1}), $q^2\sigma^2\ll1$ and hence the Zimm approximation can be used

$$\lim_{x\to0} f_D(x)=1-\tfrac{1}{3}x. \tag{5}$$

The interaction potential $V(q)$ is written as

$$V(q)=2\chi(1-\tfrac{1}{6}q^2r_0^2+\cdots), \tag{6}$$

where χ is the Flory–Huggins parameter and r_0 is in the order of σ. As the interactions are assumed to be of short range, we can identify $V(q)\simeq2\chi$, an assumption which has been verified for most polymer blends.[10] Then it follows for $S(q)$ using Eqs. (3)–(6):

$$\frac{1}{S(q)}=\frac{1}{\phi_A N_A}+\frac{1}{\phi_B N_B}-2\chi+\frac{1}{18}\left(\frac{\sigma_A^2}{\phi_A}+\frac{\sigma_B^2}{\phi_B}\right)q^2. \tag{7}$$

We set

$$\frac{\sigma_A^2}{\phi_A}+\frac{\sigma_B^2}{\phi_B}=\frac{a^2}{\phi(1-\phi)}; \tag{8}$$

further we note that χ_c the χ parameter at the spinodal is given by

$$2\chi_c=\frac{1}{\phi_A N_A}+\frac{1}{\phi_B N_B} \tag{9}$$

and hence

$$\frac{1}{S(q)}=2[\chi_c-\chi(T)]+\frac{a^2}{18\phi(1-\phi)}q^2, \tag{10}$$

where we have put all the temperature dependence of the interactions into the χ parameter in the one phase region. σ satisfies the relation $R^2=\sigma^2 N$ with R being the root-mean-square end-to-end distance. For Gauss coils, the radius of gyration is related to a the statistical segment length via $R_g^2=\frac{1}{6}a^2N$.

Now we rewrite Eq. (10) for $S(q=0)$ to get it into a standard form[32]

$$S(q=0)=\frac{1}{2\chi_c}\left(1-\frac{\chi}{\chi_c}\right)^{-1}. \tag{11}$$

It is further convenient to rewrite Eq. (10) in the Ornstein–Zernike form

$$S(q)=S(q=0)(1+q^2\xi^2)^{-1}, \tag{12}$$

where ξ is the correlation length, which is defined to be

$$\xi=\frac{a}{6}\{\phi(1-\phi)[\chi_c-\chi(T)]\}^{-1/2}. \tag{13}$$

An analogous rewriting of Eq. (12), which had led to Eq. (11), gives

$$\xi=\frac{a}{6}(4N_AN_B)^{1/4}\left(1-\frac{\chi}{\chi_c}\right)^{-1/2}. \tag{14}$$

Now we make use of the fact that our system has a lower miscibility gap, or to say an upper critical solution temperature, which means that the χ parameter will increase as the temperature is lowered towards T_c. Consequently, we assume $\chi(T)=(\chi_A/T)-\chi_B$ for the Flory–Huggins parameter, where χ_A accounts for enthalpic and χ_B for entropic interactions. The ϕ dependence is not considered because we are at $\phi=\phi_c$. Introducing this ansatz into Eqs. (11) and (14), respectively, we get

$$S(q=0)=\frac{T_c}{2\chi_A}\left(\frac{T-T_c}{T}\right)^{-1}=\text{const.}\cdot\epsilon^{-\gamma}, \tag{15}$$

and

$$\xi=\left(\frac{\chi_c}{\chi_A}T_c\right)^{1/2}C\cdot\left(\frac{T-T_c}{T}\right)^{-0.5}=\text{const.}\cdot\epsilon^{-\nu} \tag{16}$$

with $C=(a/6)(4N_AN_B)^{1/4}$ and $\epsilon=T-T_c/T$. The exponents γ and ν are the critical exponents and have the values $\gamma=1$ and $\nu=1/2$ for the mean field case and have the values $\gamma=1.24$ and $\nu=0.63$ for the Ising case.[32] In the mean field case, $2\nu=\gamma$. For the 3d-Ising case, the hyperscaling relation $(2-\eta)\nu=\gamma$ holds[32] with $\eta=0.039$. Recently, the evaluation of η by SANS from a polymer blend has been reported for the first time.[33] The derivation given is based on mean field arguments, which means that Ising exponents cannot be deduced from that. Naturally the prefactors are also not valid in the latter case. However,

relations of the type $S(q=0) \propto \epsilon^{-\gamma}$ and $\xi \propto \epsilon^{-\nu}$ with the Ising exponents are well founded by the renormalization group theory.[25,26] The experiments described here prove the range of validity of the random phase approximation, of which it is known that the crossover between mean field and Ising behavior is governed by the Ginzburg criterion.[15–17] It will be the main aim of the static part of the data evaluation to prove these scaling predictions and further prove the predictions of the Ginzburg criterion in the cited form.

B. Dynamic properties

As the system approaches the critical point, the fluctuations of the order parameter become very large as a consequence of the divergence of the generalized susceptibility of the system. For a binary mixture the order parameter is $\phi-\phi_c$, its susceptibility is given by $(\partial\phi/\partial\Delta)_{T,P}$, where $\Delta=\mu_1-\mu_2$, is the difference between the chemical potentials of the two components. The central, quasielastic component in the spectrum of scattered light is caused by the diffusive decay of the concentration fluctuations. Its decay rate Γ is given by[34,35]

$$\Gamma(q)=\frac{L(q)}{S(q)}q^2, \tag{17}$$

where L is the Onsager kinetic coefficient and S is a generalized susceptibility. As T approaches T_c, S diverges and hence Γ goes to zero, known commonly as critical slowing down. In the conventional theory[35] of critical slowing down, the Onsager coefficient is assumed to vary slowly in the critical region. Some critical coefficients, however, may change rapidly near T_c due to nonlinear couplings between the hydrodynamic modes.[22,23,36] Furthermore, the q scaling of the linewidth changes while crossing the regimes $q\xi \lesssim 1$ (called the hydrodynamical regime) and $q\xi \gtrsim 1$ (called the critical nondiffusive regime) from a q^2 to a q^3 scaling.[24] This results from the fact[37] that ξ the correlation length defined by Eq. (13) becomes comparable with q^{-1}. Fredrickson[28] has derived expressions for the mode coupling corrections to the kinetic equations by using the Kawasaki–Ohta theory[38] which is valid for mixtures of small molecules and extended it to polymer mixtures. These theoretical predictions were verified for the first time by Stepanek *et al.*[26] with some experimentally determined modifications of the ranges of the cross-over regimes between mean field to nonmean field and mode coupled to nonmode coupled. According to these modifications, most of our data refer to the regime where the dynamics of collective modes have wavelengths larger than the size of the polymer coil and the correlation length (R_g, $\xi < q^{-1}$), hence in a hydrodynamic regime. As we have investigated only one particular mixture, we did not examine various other cross-over phenomena, like Stepanek *et al.*,[18] but we focused our attention on certain scaling predictions for the critical regime including the background corrections.

The original theories by Kawasaki[24,36] and Kadanoff and Swift[23] used a mode coupled approach (coupling between the order parameter fluctuations and shear modes) to derive an expression for the linewidth that is applicable over the entire range of $q\xi$, ranging from the hydrodynamic region ($q\xi \ll 1$) up to very close to the critical point ($q\xi \gtrsim 1$). A similar expression has been derived by Perl and Ferrell[37] using a decoupled mode approach. Following the mode coupled approach, the scaled decay rate Γ^* for the critical part Γ^c, which is calculated from the measured Γ by substracting Γ^B the background part is given by

$$\Gamma^*=\frac{6\pi\eta(T)}{kT}\left(\frac{\Gamma^c}{q^3}\right), \tag{18}$$

where $\eta(T)$ is the macroscopic shear viscosity of the mixture. On the other hand, the theoretical prediction for Γ^* has the form

$$\Gamma^*=R(q\xi)\Gamma_K^*, \tag{19}$$

where $R(q\xi)$ is a weakly nonuniversal function mainly including a viscosity correction[39] and Γ_K^* is a universal function given by

$$\Gamma_K^*=\frac{K_0(q\xi)}{(q\xi)^3}. \tag{20}$$

with $K_0(x)$ being the Kawasaki function given by

$$K_0(x)=\tfrac{3}{4}[1+x^2+(x^3-x^{-1})\arctan x]. \tag{21}$$

It has the following limiting values: in the critical nondiffusive regime ($q\xi \gtrsim 1$), one gets $\Gamma^c/q^3=\text{const}$. In the hydrodynamic regime, for $q\xi \lesssim 1$, one obtains

$$\frac{\Gamma^c}{q^3}=\frac{kT}{6\pi\eta}(q\xi)^{-1}\left(1+\frac{3}{5}q^2\xi^2\right)\propto(q\xi)^{-1} \tag{22}$$

and further

$$\Gamma^c q^{-2}\propto\xi^{-1}, \tag{23}$$

a result which will be used later together with the background linewidth (Sec. V E) and finally for $q\xi \ll 1$ and $\Gamma \propto \tilde{D}q^2$, with $\tilde{D}$ being the mutual diffusion coefficient.

We had defined an Onsager coefficient $L(q)$ via Eq. (17), which can be rewritten as[31]

$$\Gamma=q^2L(q)S(q)^{-1}=L(q)q^2\left[\frac{1+q^2\xi^2}{S(q=0)}\right], \tag{24}$$

where we have assumed that $S(q)$ can be expressed by an Ornstein–Zernike form. In the limit $q\to 0$, this reduces to $\Gamma=q^2L(q)\cdot S(q=0)^{-1}$, a quantity obtained experimentally obtained for $T \gtrsim T_c$ and hence $q\xi \ll 1$.[29] Furthermore, on the basis of the dynamic random phase approximation,[40] it can be shown that the diffusive motion of a polymer (Rouse) chain is given by

$$L=\phi(1-\phi)W^0, \tag{25}$$

where W^0 is a microscopic frequency, which is related to a Rouse diffusion coefficient D_R^0 via $N\cdot D_R^0=W^0$ with N being the degree of polymerization. Thus we write for the critical part of the linewidth, by combining Eqs. (24) and (25), in the hydrodynamic regime ($q\xi \lesssim 1$)

TABLE I. The glass transition temperatures, molecular weights, indices of refraction, and densities of the polymers used in this study.

	PDMS	PEMS
T_g (°C)[a]	−125	−132
M_w (D)	20 700	33 800
M_n (D)	19 500	30 300
n_D^{20}	1.405	1.429
ρ^{25} (g cm^{-3})	0.969	0.977

[a]Determined by differential scanning calorimetry (DSC) with a heating rate of 20 K/min.

$$\Gamma^c = \phi(1-\phi)\frac{W^0 q^2}{S(q=0)}F(q\xi), \tag{26}$$

where $F(q\xi)$ is a dimensionless function. From Eq. (23), we know $\Gamma^c q^{-2} \propto \xi^{-1}$; further from Eq. (13), $S(q=0) \propto \xi^2$ hence

$$W^0 \propto \xi \tag{27}$$

by comparing Eq. (26) with Eq. (22). Obviously, the ξ dependence of the microscopic frequency and subsequently the Onsager coefficient is valid for values of ξ larger than a certain threshold, which we expect to be in the order of the radius of gyration of the polymer coil.[28,41] For ξ smaller than R_g, we interpret the Onsager coefficient along Eq. (25) and can identify it with a local, microscopic quantity. Whether this physical picture is consistent with the experimental data is a question we were interested in.

III. EXPERIMENT

A. Characterization of polymers used

The polymers were synthesized by anionic ring opening polymerization of methylcyclotrisiloxane and triethyl–trimethyl–cyclotrisiloxane yielding PDMS and PEMS, respectively, by a procedure described elsewhere.[42] The molecular weights were determined by light scattering from solution in toluene and the molecular weight distribution of the polymers was measured by gel permeation chromatography (GPC) using calibration by siloxane standards. The relevant parameters characterizing the polymeric samples are summarized in Table I. The miscibility of the blend was checked by polarization microscopy, indicating that in good agreement with the expectation $\phi_{c,\mathrm{PEMS}} = (N_{\mathrm{PDMS}}^{1/2})/(N_{\mathrm{PEMS}}^{1/2} + N_{\mathrm{PDMS}}^{1/2}), \phi_{c,\mathrm{PEMS}} = 0.465$ was found. The critical temperature T_c amounts to $\simeq 57$ °C.

B. Sample preparation

The samples suitable for light scattering were prepared by dissolving the proper amounts of polymers for a desired ϕ in n-hexane and filtration of the solution through a 0.22 μm Millipore filter into a dust-free round light scattering cell of 1/2 in. outer diameter. The solvent was removed by treatment at $T \sim 80$ °C *in vacuo* for several days.

C. Apparatus

The light scattering experiment was performed at different temperatures from $T = 57.6$ up to $T = 152.4$ °C in an angular range from $\Theta = 30°$ up to $\Theta = 140°$ using a laser light scattering goniometer (ALV-SP 81) with a custom made measuring cell which allows measurements at high temperatures. It is electrically heated with temperature control better than ±0.05 K.[43] The light source was a helium neon laser (Spectra Physics 107 A) operating at 632.8 nm with a power of 40 mW. The incident and the scattered laser beam were polarized perpendicular to the scattering plane, so that the geometry of the measurement was the so-called VV geometry. Intensities were measured using a photomultiplier operating in single photon counting mode (EMI 9863) with an accuracy of ±2% after correction for the scattering volume with the scattering angle. The full autocorrelation functions of concentration fluctuations were measured with a 128-channel correlator (Brookhaven BI 2030) in the multiple τ mode.

IV. DATA TREATMENT

A. The static structure factor

The static structure factor $S(q)$ can be obtained from the excess Rayleigh ratio $R_{VV}(q)$ due to concentration fluctuations in the blend via

$$S(q) = \frac{R_{VV}(q)\lambda^4 \bar{\rho} N_L}{4\pi^2 n^2 (\partial n/\partial\phi)^2 M_{\mathrm{mon}}} \tag{28}$$

with λ being the probing wavelength, $\bar{\rho} = \phi_A\rho_A + \phi_B\rho_B$, and n the index of refraction. For PDMS, we obtained $n(T) = 1.515\text{–}3.75 \times 10^{-4}$ T; for PEMS, $n(T) = 1.526\text{–}3.33 \times 10^{-4}$ T. $\bar{M}_{\mathrm{mon}} = \phi_A M_{\mathrm{mon}}^A + \phi_B M_{\mathrm{mon}}^B$, $(\partial n/\partial\phi)$ is the refractive index increment and is given by $(\partial n/\partial\phi) = \Delta n = (n_1 - n_2)$ because a plot of n vs ϕ is linear. To determine the increment, $n(T)$ data was used. The Rayleigh ratio $R_{VV}(q)$ is related to the measured static intensity $I(q) = \int_{-\infty}^{+\infty} I(q,\omega)\,d\omega$ via

$$R_{VV}(q) = \frac{I(q)}{I_{\mathrm{Ref}}}\left(\frac{n}{n_{\mathrm{Ref}}}\right)^2 R_{VV}^{\mathrm{Ref}}, \tag{29}$$

where Ref means reference sample. We used benzene as a reference at a scattering angle of $\Theta = 90°$ at $T = 25$ °C and $\lambda = 488$ nm; $R_{VV}^{\mathrm{benzene}} = 3.66 \times 10^{-5}$ cm^{-1}.[44] The correction for the wavelength actually used was performed according to Bender *et al.*[45] The background due to density fluctuations has been substrated according to

$$I(q)^{\mathrm{exp}} = I(q) - (\phi_A I_A^{\mathrm{density}} + \phi_B I_B^{\mathrm{density}}), \tag{30}$$

where I_A^{density} and I_B^{density} are the intensities due to density fluctuations of the pure components A and B. They are known through independent measurements. The value for PDMS is ($\lambda = 632.8$ nm, $T = 20$ °C) $R_{VV} = 4.49 \times 10^{-6}$ cm^{-1}. For PEMS, the value is $R_{VV} = 3.07 \times 10^{-6}$ cm^{-1}. Hence the correction is in the relevant temperature range at most in the order of a few percent of the totally scattered intensity.

B. The mutual diffusion coefficient

The desired normalized correlation function of the scattered electric field $g(q,t)$ is related to the measured intensity time correlation function through the Siegert relation

$$G(q,t)=\langle I(q)\rangle^2(1+f\alpha^2|g(q,t|^2) \tag{31}$$

with $\langle I(q)\rangle$ being the mean intensity. f is an instrumental factor depending mainly on the size and distance of pinholes determining spatial coherence. It is a matter of calibration.[46] The factor α is the fraction of the totally scattered intensity $I(q)$ arising from concentration fluctuations. In this case, $g(q,t)$ is identified with the concentration autocorrelation function

$$g(q,t)=\frac{\langle\phi_q(t)\phi_{-q}(0)\rangle}{\langle|\phi_q(0)|^2\rangle} \tag{32}$$

with $\langle|\phi_q(0)|^2\rangle$ being the mean-square concentration fluctuations. We further identify[29]

$$g(q,t)=\frac{S(q,t)}{S(q)} \tag{33}$$

with $S(q,t)$ being the dynamic structure factor and $S(q)$ is given by Eq. (28). The relaxation time of $S(q,t)$ is given via

$$S(q,t)=S(q,t=0)\exp(-\Gamma t) \tag{34}$$

with Γ being the measured Rayleigh linewidth. It is related to an apparent mutual diffusion coefficient $\tilde{D}$ via $\Gamma=\tilde{D}q^2$.

C. Multiple scattering

Possible multiple scattering from our system was estimated according to $I_{\text{meas}}=I\exp(-\tau_D d)$ with τ_D being the turbidity of the solution and d the light path length. τ_D was estimated according to Chang *et al.*[47] and amounted to $\sim 2.5\%$ at a temperature for which $q\xi=1$. For $q\xi=0.6$, the correction would be less than 0.1%. Hence no multiple scattering correction was undertaken.

V. RESULTS AND DISCUSSION

A. The static structure factor

According to Eq. (10) a plot of $S(q)^{-1}$ vs q^2 should give straight lines if the Zimm approximation is valid. $S(q)$ is related to $R_{VV}(q)$ via Eq. (28). In Fig. 1, a corresponding plot is shown for a series of temperatures, the lowest one being only a few degrees above the spinodal temperature. Obviously, the data is well represented by Eq. (10). Furthermore we note the more or less constant slope which is given by $a^2/18\phi(1-\phi)$. In a first approximation, here only the temperature dependence of the coil flexibility enters which is a small effect in the observed temperature interval. Moreover, the constant slope indicates[10] the absence of a spatial structure of the interaction parameter $\chi(T)$. Then, according to Eq. (6), we can safely set $V(q)\simeq 2\chi$ and consequently determine $2[\chi_c-\chi(T)]$ from the intercept of Fig. 1 for $q=0$. The static structure factor $S(q=0)$ is given by

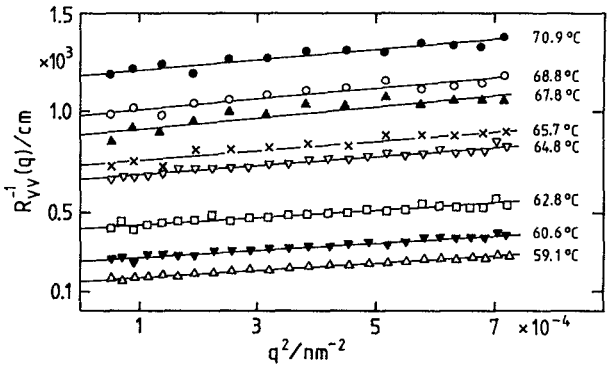

FIG. 1. The inverse Rayleigh ratio $R_{VV}(q^{-1})$ vs the square of the scattering vector q^2 (Zimm plot) according to Eq. (8) for various temperature in degrees Celsius as indicated.

$$\frac{1}{S(q=0)}=2[\chi_c-\chi(T)] \tag{35}$$

determining $\chi(T)$. In Fig. 2, we have plotted the resulting $\chi(T)$ for $\phi_{C,\text{PEMS}}=0.465$ and $\phi_{\text{PEMS}}=0.18$ as a function of the inverse absolute temperature. According to the picture of a Flory–Huggins interaction parameter,[13,31] we expect a straight line. The linear fit to the ansatz $\chi(T)=(\chi_A)/(T)-\chi_B$ gives the values for the system specific constants χ_A and χ_B as listed in Table II. However, as can be seen from Table II, there is a strong ϕ dependence of χ, which we will not consider here because we only consider[48] $\phi=\phi_c$. Since the χ parameter is a mean field quantity, we have used only $S(q=0)$ in the mean field regime calculating $\chi(T)$ for $\phi=\phi_c$. It is convenient to plot $S(q=0)^{-1}$ vs $1/T$ because of the form of Eq. (15). The result is shown in Fig. 3. From this plot, two important features emerge. First, over a very broad temperature range, the data points fall on a straight line; second, close to $1/T=3\times10^{-3}$ K^{-1}, we observe a deviation towards the critical point, which we have

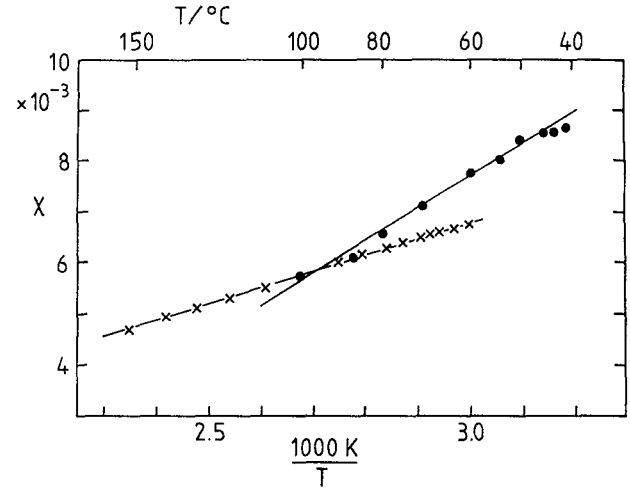

FIG. 2. The Flory–Huggins interaction parameter χ as a function of the inverse temperature. Shown is $\chi(T)$ for the critical $\phi_{C,\text{PEMS}}=0.465$ (×) and a $\chi(T)$ for a $\phi_{\text{PEMS}}=0.18$ (●) at the edge of the phase diagram.

TABLE II. Enthalphic and entropic parts of the Flory–Huggins parameter $\chi(T)$ for the three different volume fractions ϕ studied, including the critical $\phi_c=0.465$.

ϕ_{PEMS}	χ_A	χ_B
0.18	6.42	11.54×10^{-3}
0.465	3.22	2.90×10^{-3}
0.70	4.52	6.95×10^{-3}

indicated with an arrow as T_c^{-1}. Through the data at more elevated temperatures we have drawn a straight line which is extrapolated to $S(q=0)^{-1}=0$ to give the fictive mean field critical temperature $T_{c,MF}$ = 59.5 °C. However, the critical exponent cannot be determined from Fig. 3, but we have to use Eq. (15) in a double logarithmic form such that $\log S(q=0)$ vs $\log[(T-T_{c,MF})/T]=\log\epsilon$ should give a linear plot with slope $\gamma=1$ the mean field exponent. This behavior is shown in Fig. 4. The derivation of Eq. (15) is based on the mean field arguments, thus the prefactor $T_c/2\chi_A$ which is known independently (cf. Table II) is obtained by the extrapolation of the data points towards $T\to\infty$. However, for a temperature corresponding to $\log\epsilon \simeq -2$, we observe a deviation from the mean field behavior, which is in agreement with the qualitative finding shown in Fig. 3. The crossover from mean field to an Ising behavior can be tested strictly by plotting $\log S(q=0)$ vs $\log(T-T_{c,I}/T)$ with an Ising critical temperature. We got a good result with $T_{c,I}=56.5$ °C and $\gamma=1.24$, the correct Ising critical exponent, shown in Fig. 5. All the data points could now be linearized in the relevant temperature range close to T_c. However, one may argue that there is a need for two different types of theoretical approaches (mean field approach vs 3d-Ising model) to describe the whole set of data. Furthermore the Ising exponents are not derived consistently by Eqs. (15) and (16). One may look on that

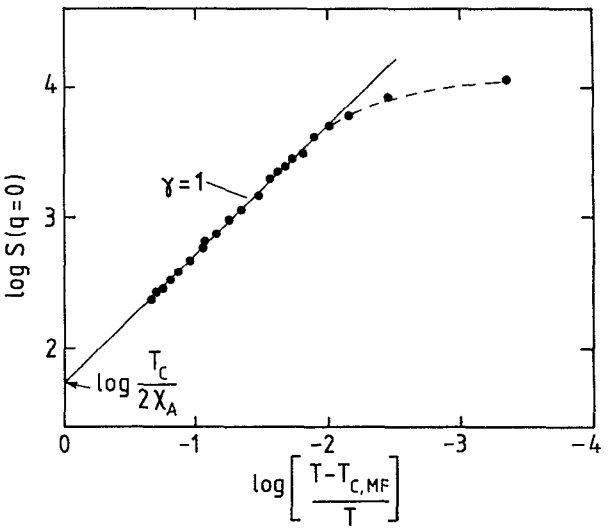

FIG. 4. The logarithm of the structure factor $S(q=0)$ vs the logarithm of the reduced temperature with the mean field T_c according to Eq. (13) showing the mean field exponent $\gamma=1$. The value of the intercept $T_c/2\chi_A$ is indicated by the arrow.

from two different points of view. The data analysis presented here focusses on the limits of the random phase approximation, the other point of view may be to use a unified theory[49–51] which is able to realy model the observed crossover and by that simply circumvents the mean field argumentation.

B. The correlation length

According to Eq. (12) a plot of $S(q=0)/S(q)$ vs q^2 should result in straight lines. From the slopes, the determination of the correlation length ξ is possible. Such an Ornstein–Zernike plot is shown in Fig. 6 for various temperatures. Qualitatively, one sees that for $T\to T_c$, the cor-

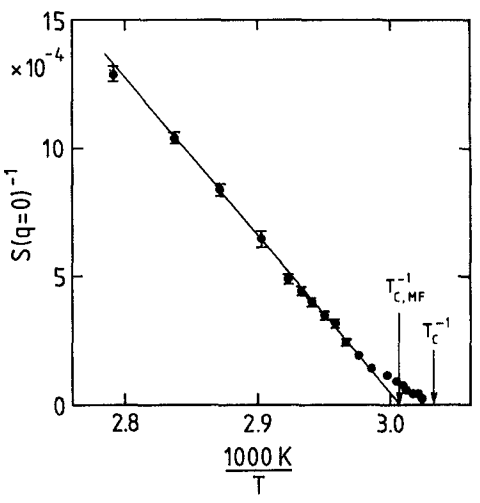

FIG. 3. The inverse structure factor for $q=0$ vs the inverse temperature. For temperatures close to the critical point, the error bars are smaller than the symbols used. $T_{c,MF}$ is the extrapolated mean field critical temperature from this plot and T_c is the critical temperature from phase contrast microscopy.

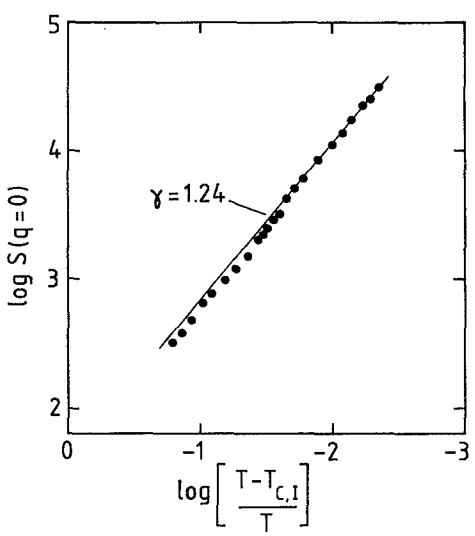

FIG. 5. The logarithm of the structure factor $S(q=0)$ vs the logarithm of the reduced temperature with the Ising T_c according to Eq. (13) showing the Ising exponent $\gamma=1.24$.

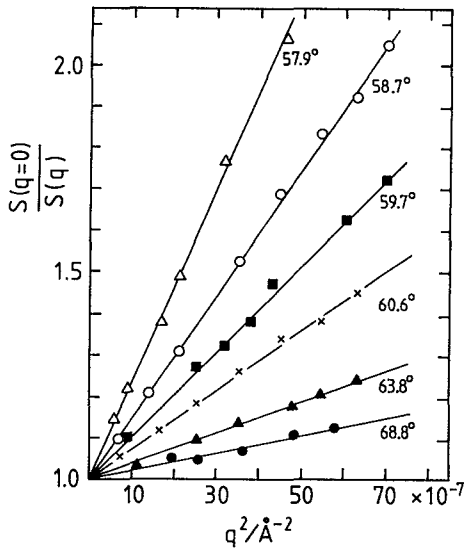

FIG. 6. The Ornstein–Zernike plot of the data for various temperatures above the critical point in degrees Celsius as indicated according to Eq. (12). From the slope, the correlation length is calculated.

relation length tends to diverge. In principle, we expect the same deviations from mean field theory for $\xi(T)$ as we had already discussed for $S(q=0)$ as a function of temperature. In Fig. 7, a double logarithmic plot according to Eq. (16) is shown, giving $\nu=0.5$, the correct mean field critical exponent and further, deviations from this behavior at the same temperature difference to T_c as in the case of the structure factor. Accordingly a plot with the Ising critical temperature (Fig. 8) results in a linearization of the correlation length data with the correct Ising critical exponent $\nu=0.63$. As the derivation of Eq. (16) is based on the random phase approximation, we determine $\lim_{T\to\infty}\xi=\xi_0$ from Fig. 7 to give $\xi_0=20.4$ Å. On the other hand, the value is given by $\xi_0=\frac{1}{6}a\sqrt{2}(N_AN_B)^{1/4}[(\chi_C/\chi_A)T_c]^{1/2}$, where a is defined by Eq. (8). Since for PDMS $\sigma=5.83$ Å,[52] we

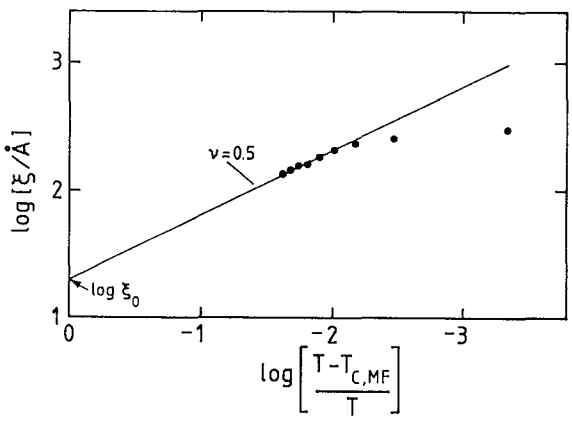

FIG. 7. The logarithm of the correlation length ξ vs the logarithm of the reduced temperature with the mean field T_c according to Eq. (16) showing the mean field exponent $\nu=0.5$. The value of the intercept ξ_0 is indicated by an arrow.

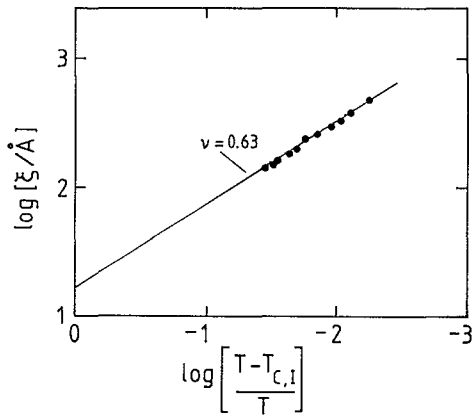

FIG. 8. The logarithm of the correlation length ξ vs the logarithm of the reduced temperature with the Ising T_c according to Eq. (16), showing the Ising exponent $\nu=0.63$.

can estimate $\sigma_{\mathrm{PEMS}}=6.4\pm0.3$ Å. This is not very precise because of the very sensitive extrapolation, but definitely gives the right order of magnitude.

C. The Ginzburg criterion

From Fig. 4, we can estimate the width of the temperature interval describing the deviations from the mean field behavior as being $\Delta T=6$ K. The classical Ginzburg criterion predicts that the crossover takes place if the fluctuations of the order parameter become comparable with the order parameter itself.[13,31] If that is properly worked out, then for the case of interest here, following the papers by de Gennes[15] and Joanny,[16] one gets

$$\Delta T\simeq\frac{T_c}{N} \tag{36}$$

for the width of the transition zone. Obviously this gives $\Delta T\sim1$ K which is almost one order of magnitude too small. This seems to be a general finding since in all published experimental data concerning this point (so far only by SANS),[7,14,17,18] ΔT via Eq. (36) is wrong in one direction—it is too small. Recently Bates *et al.*[17,18] have proposed a new relation, which is an extension of Joanny's work,[16] taking into account the case $N_1\neq N_2$ and $a_1\neq a_2$. It reads

$$\epsilon=Cv_m^2 \times\frac{[1/(N_1\phi_1^3)+1/(N_2\phi_2^3)]^2}{[1/(N_1\phi_1)+1/(N_2\phi_2)][R_1^2/(N_1\phi_1)+R_2^2/(N_2\phi_2)]^3}, \tag{37}$$

where $\epsilon=(\chi_{c,\mathrm{MF}}-\chi)/(\chi_{c,\mathrm{MF}})$, v_m is the segment volume, and $R_i^2=\frac{1}{6}N_ia_i^2$. It is claimed further that C is a system-independent constant in the order of 0.3. We rewrite Eq. (37) for our purpose

$$\frac{1}{T_c}-\frac{1}{T}=\text{const.}\cdot Cv_m^2, \tag{38}$$

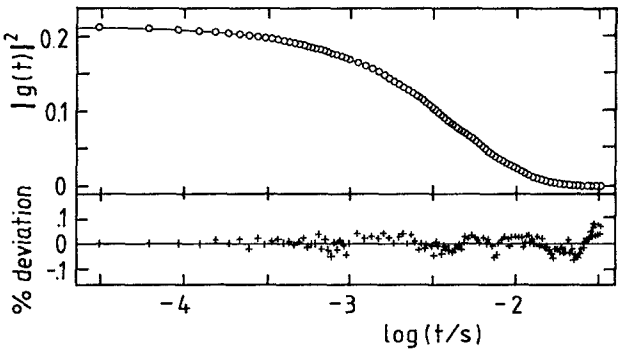

FIG. 9. (Upper part) The nonnormalized intensity autocorrelation function of concentration fluctuations at $T=81$ °C for a scattering angle of $\Theta=90°$. The full line is a fit of Eq. (34) to the data (○). (Lower part) The deviations of the single exponential fit from the experimental points in percent.

where the constant contains all N, ϕ, R, and χ factors.

Using a geometric mean for $\bar{v}_m[v_m=M_w/(N\cdot\rho)]$, we obtain $\bar{v}_m=83.8$ cm^3 mol which is $\bar{v}_m=1.39\times10^{-22}$ cm^3. Then we get along Eq. (38) $C=0.346$, which is close to the universal value proposed by Bates *et al.*[17,18] We indeed feel that Eq. (37) is substantial progress as it, for the first time, allows the quantitative description of data of this kind.

D. The mutual diffusion coefficient

In Fig. 9, a typical concentration autocorrelation function is shown, in which a single exponential decay function according to Eq. (34) has been fitted. The resulting, very small deviations to this fit are shown further in the lower part of Fig. 9. We have found that every measured correlation function exhibited a single exponential time decay behavior as depicted along Eq. (34) with similar small deviations illustrated in Fig. 9. When $T\to T_c$, the q scaling of Γ (for $T\gg T_c$, $\Gamma=\tilde{D}q^2$) changes to a q^3 scaling according to the arguments given in the section on theoretical aspects of the dynamics. This is shown qualitatively in Figs. 10(a) and 10(b). The foregoing arguments in mind, we have plotted in Fig. 10(a) according $\Gamma=\tau^{-1}\propto q^{\alpha}$, where α changed from 2 to 3 for $T\to T_c$. Exponents α, determined by linear least-squares fit, as shown in Fig 10(a), are plotted vs temperature in Fig. 10(b) to show the predicted change. Clearly the value of 3 is almost reached for T close to T_c. Furthermore, one notices a relatively broad temperature range in which we have departures from the q^2 scaling. That relatively broad temperature range is due to the large prefactor of the static correlation length. If we proceed in our phenomenological description at this point, we can calculate an apparent $\tilde{D}$ from all this data according to Eq. (34). This set of data of $\tilde{D}$ is plotted vs T^{-1} in Fig. 11 for three different compositions, including the critical $\phi_c=0.465$, which we investigate here mainly. Clearly, the so-called "critical slowing down" for $T\to T_c$ is observed. A similar observation as has been reported by Green and Doyle[53] for the system PS/*d*-PS by elastic forward recoil spectroscopy and by Kanetakis and Fytas[54] using quasielastic light scattering results of the system PEO/PPO.

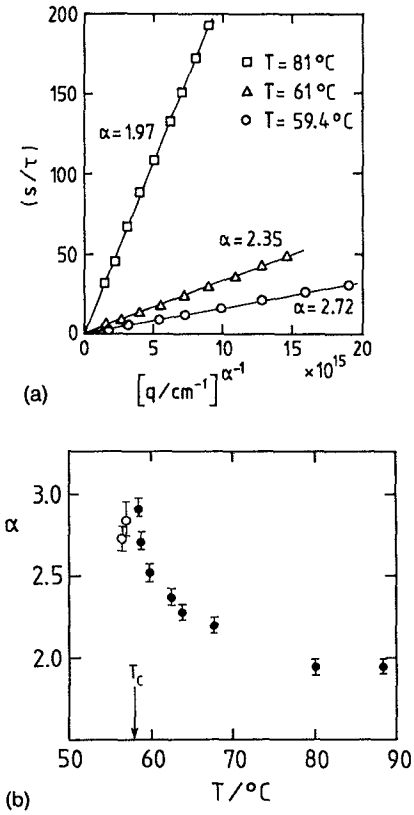

FIG. 10. (a) The inverse of the characteristic decay time of concentration fluctuations vs the momentum transfer to the power of α. (b) The exponent α, as determined exemplarily via (a), vs temperature (●). The critical temperature is indicated with an arrow. Two points for $T<T_c$, where dynamics due to phase separation takes place, are also given (○).

Moreover by closer inspection of Fig. 11, one notices that also for $\phi=0.7$, the onset of a critical slowing down appears before the binodal has been reached. It is indicated by the dashed vertical lines and prevents from measuring further down with temperature. The critical slowing down can be interpreted qualitatively using Eqs. (24), (25), and (35) for $q\xi\ll1$,

$$\tilde{D}=2\phi(1-\phi)(\chi_c-\chi)W^0 \tag{39}$$

and hence $\tilde{D}$ has to vanish for $\chi\to\chi_c$, since all other quantities remain finite. Rewriting Eq. (39) leads to

$$W^0=\frac{\tilde{D}\cdot S(q=0)}{\phi(1-\phi)}, \tag{40}$$

where the microscopic frequency W^0, related to the Rouse diffusion coefficient in the case of nonentangled polymer chains, can be calculated easily from measurable quantities (cf. Sec. V B). The result for W^0 as a function of the inverse temperature is shown in Fig. 12. From the plot, one sees that W^0 behaves regularily at higher temperatures which means that its dynamics becomes slower by lowering the temperature; furthermore we can fit a straight line at temperatures above $T\simeq90$ °C to the data points leading to an activation energy of $E_a=8.2$ kcal/mol. Lowering the temperature leads to an acceleration of W^0, which cannot be understood on the basis of the mean field expression along Eq. (40). We furthermore tried to use Eq. (24) for

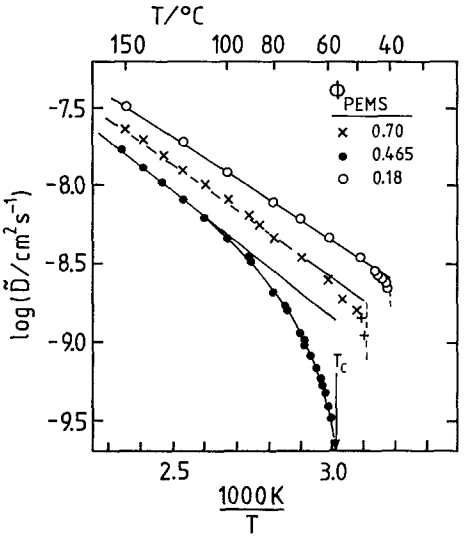

FIG. 11. An Arrhenius plot of the apparent mutual diffusion coefficient for three different compositions of ϕ_{PEMS}, including the critical ϕ (●). The critical temperature is indicated by an arrow. Dashed lines indicate the binodal temperatures for $\phi \lesssim \phi_C$, as determined by phase contrast microscopy.

$q\xi \lesssim 1$, which basically replaces $S(q=0)$ by $S(q)$ using the Ornstein–Zernike form, but of course that did not remove the circumstance that W^0 turns to accelerate by lowering $T \to T_c$. Indeed this fact needs to be analyzed in terms of mode coupled expressions.

E. The critical linewidth

The theories developed[22–26] to describe the critical behavior of transport properties near the critical point apply only to the "critical" part of the transport property. Therefore the noncritical background part of the measured transport coefficient (the diffusion in the case of binary mixtures) has to be subtracted. We write

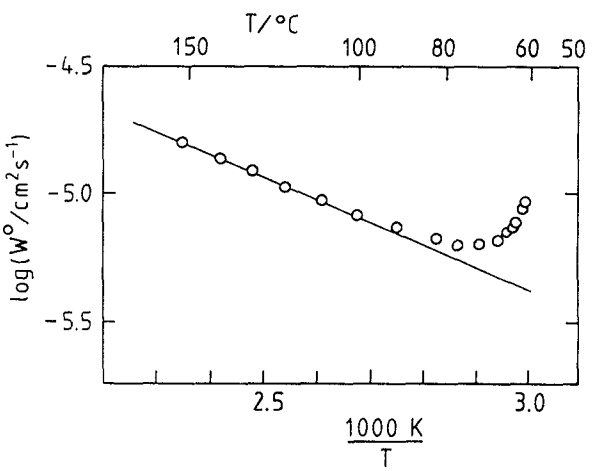

FIG. 12. An Arrhenius plot of the microscope frequency W^0 as calculated by Eq. (40).

$$\Gamma^{meas} = \Gamma^C + \Gamma^B, \tag{41}$$

where C denotes the critical and B the background part of the measured (meas.) linewidth, which is defined by Eq. (17). The proper treatment of the background part is discussed thoroughly by Swinney and Henry[34] and Oxtoby and Gelbart.[55] If one assumes, following these authors, that the susceptibility (S) can also be written as a sum of background (S^B) and critical (S^C) parts, then we can write with the help of Eq. (17) assuming that $S^B \ll S^C$ for $q\xi \lesssim 1$,

$$\Gamma^{meas} = \frac{L(q)}{S(q=0)} q^2(1+q^2\xi^2) + \Gamma^C. \tag{42}$$

However, this separation is somewhat arbitrary. The use of the proposal by Swinney and Henry[34] leading to Eq. (42) is not the only possible way of handling Eq. (41). Other methods are described and discussed in the literature.[56] If we accept Eq. (42) as a working equation, we then see, by comparing it with Eq. (24), that the critical part of the linewidth can be calculated if we extract the background part along Eq. (24). If this is a correct procedure, it can be crosschecked using a relation for the ratio of Γ^B to Γ^C which is given by Oxtoby and Gelbart.[55] It reads

$$\frac{\Gamma^B}{\Gamma^C} \simeq \frac{3}{4} \frac{1}{q_D \xi_0} \left(\frac{T-T_c}{T} \right)^{\nu}, \tag{43}$$

where q_D is an adjustable parameter in the Perl–Ferrell theory[37] (the Debye cut-off wavenumber, where the mode coupling contributions disappear) and ξ_0 is given formally by $\lim_{T \to \infty} \xi(T)$ taken from Fig. 8. For T_c the Ising critical temperature is used. Following Perl and Ferrell[37] again, we can estimate q_D via

$$q_D \simeq \frac{CkTq^2}{8\pi\eta^B \Gamma_0^B \xi_0^2}, \tag{44}$$

where C is a constant in the order of unity[55] ($c \approx 0.9$) and η^B is the background part of the macroscopic shear viscosity of the mixture, and Γ_0^B is given by

$$\Gamma^B = \Gamma_0^B \left(\frac{T-T_c}{T} \right)^{\gamma}, \tag{45}$$

where to the power of γ in Eq. (45) follows immediately from Eq. (43) remembering Eq. (23). In our data evaluation process, we proceeded in the following way, asking ourselves, what is the physical meaning of the Debye cutoff q_D? We argue that $q_D \simeq R_g^{-1}$, as already stated in the theoretical chapter, because if $\xi \ll R_g$, then coupling of modes or to say interaction between different coils is no longer sensible. We tried in a first self-consistent way to calculate Γ^B/Γ^C via Eq. (43) using $a=6$ Å and $\xi_0=20$ Å, further inserting the Ising T_c and $\gamma=0.63$. Both ways to calculate Γ^B and Γ^C [either via Eq. (42) with the help of Eq. (24) or using Eq. (43) assuming a physically reasonable q_D which is justified via Eqs. (44) and (45)] lead to identical results within the experimental error. This result of the separation is shown in Fig. 13. One sees that the prediction of Eq. (23) $\Gamma^C q^{-2} \propto \xi^{-1}$ is correct; furthermore, we also find roughly $\Gamma^B \propto \epsilon^{\gamma}$ ($\gamma=1.2$ instead of 1.24). From the extrap-

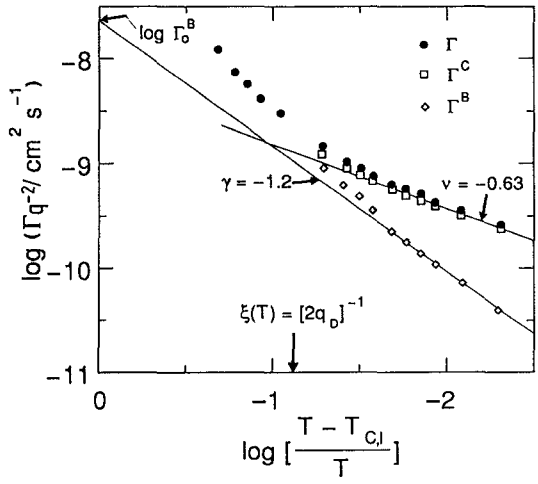

FIG. 13. The logarithm of the measured Rayleigh linewidth Γ_q^{-2} (●) vs the reduced temperature with the Ising critical temperature. The separation of Γ into the background part Γ^B (◇) and the critical part Γ^C (□) is shown with the critical exponents ν [Eq. (23)] and γ [Eq. (44)], respectively. The meaning of log Γ_0^B and $\xi(T)=(2q_D)^{-1}$ is discussed in the text.

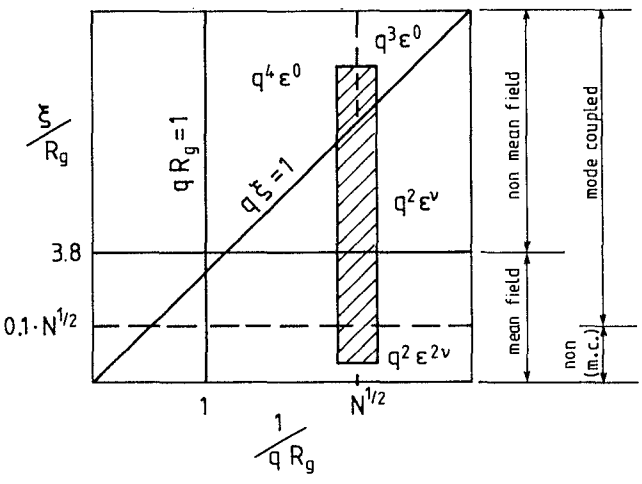

FIG. 14. A schematic diagram after Ref. 18 showing the crossover between mode coupled to nonmode coupled and mean field to Ising, respectively. The range for our sample under study is indicated by the bar.

olation of the background linewidth to infinite temperatures, we furthermore get $\Gamma_0^B q^{-2}=10^{-7.6}$ cm^2/s. If we put this value back into Eq. (44) together with η^B, which we assume to be the macroscopic shear viscosity since $\eta^C \ll \eta_S(T)=\eta^B$ in the temperature range of interest,[55] we indeed get $q_D=1.33\times10^{-2}$ Å^{-1} which is almost $0.5R_g^{-1}=1.15\times10^{-2}$ Å^{-1}. That means, it is a legitimate way of self-consistent data treatment.

F. Mean field vs Ising critical dynamics

In the following discussion on the possible crossover between mode coupled to nonmode coupled dynamics and mean field to Ising, respectively, we refer to the findings by Stepanek *et al.*[18] who have experimentally modified Frederickson's work.[28] For reasons of clearness, we adopt a similar diagram to that of Stepanek *et al.*,[18] which is shown by Fig. 14. The ordinate of the diagram represents the inverse temperature. Going up means approaching T_c. We see that our sample measured lies on the abscissa roughly symmetrically around $N^{1/2}$, due to variations in q. As can be seen from the Fig. 14, most of our data was accomplished in a dynamic region where $\Gamma^c \propto q^2\epsilon^\nu$, which is called the hydrodynamic regime. This is essentially the prediction of Eq. (23), namely that $\Gamma^c \propto q^2\xi^{-1}$ since $\xi \propto \epsilon^{-\nu}$ because of Eq. (16). Close to T_c, we expect a crossover to the critical nondiffusive regime, where basically the linewidth will not depend on temperature. For $T \gg T_c$, another crossover is expected, the mode coupled to mode decoupled crossover. Let us first concentrate on these various crossover phenomena and not on the mean field to Ising crossover.

To illustrate this, Γq^{-2} vs the reduced temperatures with a mean field T_c [Fig. 15(a)] and an Ising T_c [Fig. 15(b)] is plotted. Thereby we use for simplicity reasons not Γ^C, but the directly measured Γ, which produces in the hydrodynamic regime ($-1 < \log\epsilon \lesssim -2.2$, depending on q) only a negligible error, as can be seen from Fig. 13. From Figs. 15(a) and 15(b), a range of ϵ can be found where the correct exponents can be fitted to the data according to $\xi^{-1} \propto \Gamma^c q^{-2}$ [cf. Eq. (23)], i.e., $\nu=0.5$ for the mean field case and $\nu=0.63$ for the Ising case. Deviations from the dynamic scaling prediction [Eq. (23)] occur in both cases roughly at about $\log\epsilon \simeq -1$. This latter point is in agreement with the findings by Stepanek *et al.*[18] (Fig. 14). They have found that the crossover between mode coupled to nonmode coupled dynamics is governed by the value $0.1\ N^{1/2}=\xi/R_g$ hence for our system $1.73\ R_g=\xi$. The temperature for which $\xi=73$ Å is exactly at $\log\epsilon=-1$ (cf. Fig. 8). The position is indicated by an arrow in Fig. 15(b). This is an important finding because we have found that it is the value of $q_D^{-1} \simeq 2R_g$, which determines the crossover between mode coupled and mode decoupled dynamics as can be seen in Fig. 13. This particular value was introduced since the polymer coil is more space filling than given by R_g. So we set arbitrarily the length being twice that value to assure that it is now a distance where the form factor has come down. Consequently, we can identify this value $(2q_D)^{-1}$ being the modified predicted crossover from mode coupled to nonmode coupled dynamics,[18] which is given by $0.1\ N^{1/2}R_g$ as shown in Figs. 15(b) and 14, respectively, for our system. That means physically that the background corrections for the critical dynamics in polymer mixtures are not as important as for small molecules, but of course not negligible, especially if one is interested in scaling predictions along Eqs. (23), (27), and (46). Also, the determination of a correct q_D is not possible without that analysis; furthermore the exact knowledge of Γ^c is important for calculating the Kawasaki shape function (cf. Sec. V G). Examining Fig. 15(b) further, we find at $\log\epsilon \simeq -2.2$ the cross-over form $\Gamma^c \propto \epsilon^\nu$ to $\Gamma^c \propto \epsilon^0$. It is governed through the condition $q\xi \gtrsim 1$. For $\log\epsilon=-2.2$, we have $\xi=570$ Å (cf. Fig. 8), hence $q\xi=1.2$ is reached with $\lambda=632.8$ nm at $\theta=90°$ scattering angle. For values

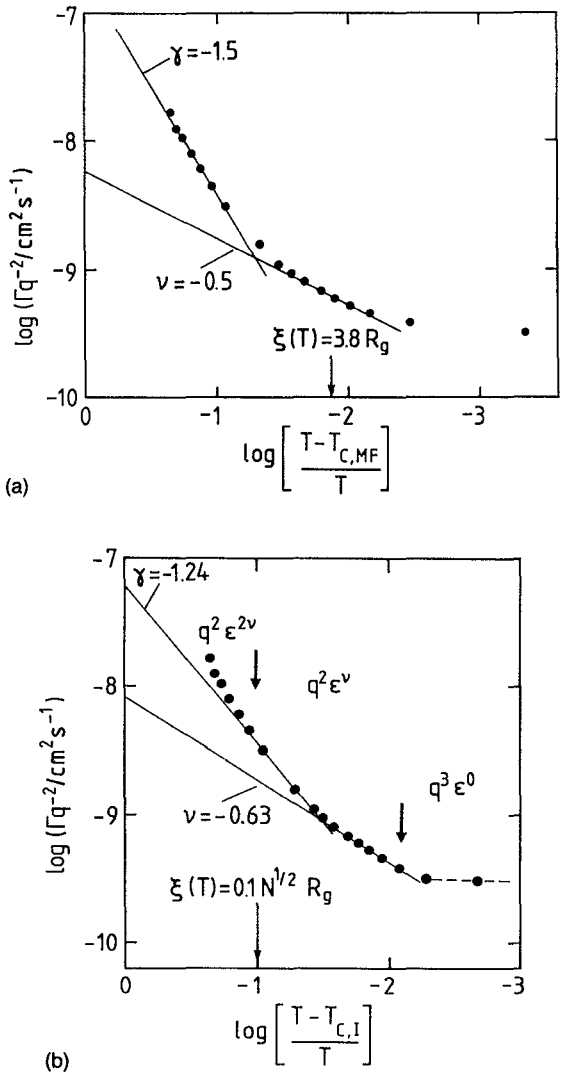

FIG. 15. (a) The logarithm of the Rayleigh linewidth Γ_q^{-2} vs the reduced temperature with the mean field critical temperature according to Eq. (23), showing the mean field exponent $\nu=0.5$. The crossover between mean field to nonmean field behavior is indicated by the arrow as derived from static properties [Eq. (37)]. (b) The same as (a), but the reduced temperature with the Ising critical temperature, showing the Ising exponent $\nu=0.63$. The crossover between mode coupled to nonmode coupled dynamics according to the modification of the theoretical result (Ref. 28) by Stepanek *et al.* (Ref. 18) is indicated by an arrow. The predicted crossover (cf. Fig. 14) between the hydrodynamic regime and the critical nondiffusive regime at $\log \epsilon = -2$ is also indicated.

for $\log \epsilon < -1.2$ from Fig. 15(a), we see the crossover from $\Gamma^c \propto \epsilon^\nu$ to $\Gamma^c \propto \epsilon^{2\nu}$ according to Fig. 14. The slope we determine in this regime is $\gamma=1.5$ instead of $2\nu=\gamma=1$ with the mean field exponents. We have chosen the mean field representation in Fig. 15(a) because for $T \gg T_c$ the mean field description is adequate to describe the system behavior. However, if we use the Ising representation in Fig. 15(b) over the whole temperature range, we find a slope of $\gamma=1.44\pm0.1$ instead of $\gamma=1.24$ in the mode decoupled regime. This seems to shed some light on the possibility of describing the whole set of data by a unified theory,[49–51] where only Ising exponents occur. Then note that the somewhat artificial discrimination between mean field and Ising critical behavior is removed and may help to remove the statement in Stepanek's paper,[18] that it is theoretically not understood why the mean field to Ising crossover occurs well in the mode coupled regime and not vice versa as comes out in Fredrickson's work.[28]

Now let us turn to the crossover between mean field to nonmean field which is of further interest. The mean field description can be applied down to $\log \epsilon \simeq -2.2$ with $T_{c,\mathrm{MF}}$ [see Fig. 15(a)] which are the points down to $\log \epsilon \simeq -1.9$ with $T_{c,I}$ in Fig. 15(b). There ξ is about 240 Å (cf. Fig. 8) being far in the mode coupled regime. This behavior is in qualitative agreement with the findings by Stepanek *et al.*[18] who claim that the mean field to nonmean crossover should occur at $\xi/R_g \simeq 2.2$ based on a constant $C=0.21$ in Eq. (37). We have found $C=0.346$ (cf. Sec. V C) which means that our crossover from mean field to nonmean field behavior should occur at $\xi(T)/R_g=3.8$, which is indicated by an arrow in Fig. 15(a). Consequently we have drawn a line at $\xi/R_g=3.8$ in Fig. 14 to indicate this latter crossover. If we inspect Fig. 15(a) more closely, we find, however, a deviation in the determination of the cross-over temperature from static properties, which had led to $C=0.346$ in Eq. (37) and from dynamic properties, shown in Fig. 15(b). There the crossover seems to occur at a temperature somewhat closer to $T_c(\log \epsilon \simeq -2.2)$. These findings are similar to those by Stepanek *et al.*,[18] but there is no explanation as yet.

G. Comparison with the Kawasaki function

Having calculated the critical part of the Rayleigh linewidth via Eq. (41), we can determine the scaled linewidth Γ^*, given by Eq. (18). For that purpose, we need to know the macroscopic shear viscosity of the mixture. Since we did not measure it, we calculated $\eta(T)$ from the shear viscosities of the pure components A and B assuming thereby $\eta_{\mathrm{mix}}^{-1}=\phi_A\eta_A^{-1}+\phi_B\eta_B^{-1}$. We have used $\eta_{\mathrm{PDMS}}=\exp\{[(1.92\times10^3)/T]-0.97\}$ (Ref. 57) and for $\eta_{\mathrm{PEMS}}=\exp\{[(2.46\times10^3)/T]-1.24\}$ (Ref. 42) with η in counterpoise. However, the given expressions are only valid in the high temperature regime, which can be seen from the Arrhenius type of activation energy. This would not be true in the vicinity of the glass transition temperature. We have used angular-dependent measurements of the Rayleigh linewidth in the temperature range $T=58.8$ up to $T=69.1$ °C; furthermore some data points at a fixed scattering angle $\theta=90°$ at higher temperatures up to $T=91$ °C, which determined the possible q range and range of Γ^C. For values of $T<61$ °C, only data at scattering angles $\theta<90°$ were taken to make sure that the condition $q\xi \simeq 1$ is fulfilled. On the other hand, Eq. (19) gives the theoretical expression for the scaled linewidth, for which ξ the static correlation length is needed. We took values for ξ from Fig. 8. In Fig. 16, the result of the numerical calculation of the theoretical curve given by Eq. (19) [with the help of Eqs. (20) and (21)] is given as a full line. The experimental data, determined by Eq. (18), fall on the theoretical curve. As was already stated by Hamano *et al.*,[20] it is due mainly to the large prefactor of $\xi(T)$ that we could reach values for $q\xi \simeq 2.5$, being well in the critical nondiffusive

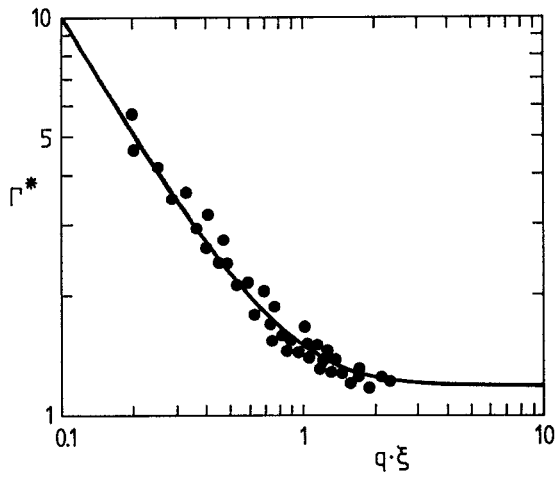

FIG. 16. Scaled linewidth Γ^* vs $q\xi$. The full line is the theoretical prediction [Eq. (19)]; experimental points (●) are determined by Eq. (18).

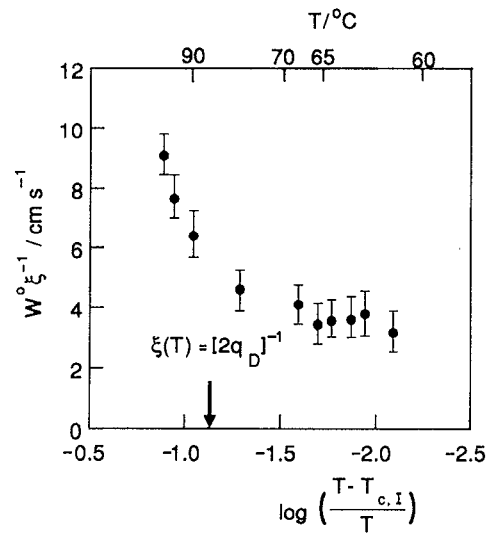

FIG. 17. The ratio of W^0 and ξ vs the reduced temperature with the Ising T_c. From the temperature on where ξ becomes larger than a certain threshold ($\simeq 2R_g$), the ratio is constant according to Eq. (27).

decay regime, although no extreme experimental efforts have been undertaken to go as close as possible to the critical point. In the latter regime, the agreement between theory and experiment was enhanced largely using the viscosity correction $R(q\xi)$ [cf. Eq. (19)] which we took numerically from the paper by Kawasaki and Lo.[39] Due to errors in the determination of the background, it is difficult to differentiate conclusively between the mode coupled expressions[23,24] and those given by the renormalization group approach.[25,26] The latter one gives a factor of $(1\text{–}2)^{-1}$ times the right-hand side of Eq. (18). However, the deviations between theory and experiment in Fig. 16 are quite random, therefore, we feel that the mode coupled expression describes it a little better.

H. The microscopic Rouse frequency

The result for W^0, calculated via Eq. (40) as a function of the inverse temperature is shown in Fig. 12. Now we turn to the regime between T_c and $T=90$ °C in Fig. 12, where W^0 starts to accelerate. According to Eq. (27), we should expect $W^0 \propto \xi$ in this regime, or $W^0/\xi = \text{const.}$, which we have plotted in Fig. 17 vs the reduced temperature with the Ising critical temperature. Indeed, considering the error bars, this is correct. A small error is buried in the approximation to simplify the term $(1+\frac{3}{5}q^2\xi^2)$ in Eq. (22) by a dimensionless function $F(q\xi)$ which is then used in Eq. (26) to calculate $F(q\xi)\cdot S(q=0)^{-1}$ being $S(q)$ in the Ornstein–Zernike approach. Since $F(q\xi)$ is dimensionless, it does not change the proportionality shown in Fig. 16. Comparing Eqs. (22) and (26), the Stokes–Einstein equation comes out as it should. The relation reads

$$\Gamma^c q^{-2} = \frac{kT}{6\pi\eta\xi_D} \tag{46}$$

and is used to define the dynamic correlation length ξ_D. We have calculated ξ_D in the hydrodynamic regime R_g, $\xi < q^{-1}$ and have compared it to ξ the static correlation length given by Eq. 16 (cf. Fig. 8). For the ratio of ξ_D/ξ, we find in the cited regime a constant value of 1.02 ± 0.12, in contrast to Stepanek *et al.*[18] who find a constant ratio $\xi_D/\xi = 0.6$, but in agreement with findings for simple systems.[58]

Now we will concentrate on the high temperature data for $T > 90$ °C in Fig. 12 for $\log \epsilon > -1.2$ in Fig. 17. If the behavior of W^0 can be understood as a local, microscopic quantity, then its calculation from independent mechanical measurements, assuming the validity of the Rouse model, should be possible. For that purpose, we have used the data of the shear viscosity η_0 (cf. Sec. V F), which is related to the monomeric friction coefficient ζ_0 on the basis of the modified Rouse theory[59] via

$$\eta_0 = \frac{\zeta_0 \rho a^2 N_L M}{36 M_{\text{mon}}^2} \tag{47}$$

with M_{mon} being the momomer molecular weight. All other symbols have the usual meanings. The question now is how to treat a mixture in terms of a mean friction coefficient $\langle \zeta^{\text{mix}} \rangle$ if only ζ_0 for the pure components are known. For this particular system, we know from measurement[60] of a mixture PDMS($N=80$)/PEMS($N=90$) that an empirical relation

$$\frac{\phi_A}{\zeta_A} + \frac{\phi_B}{\zeta_B} = \frac{1}{\langle \zeta^{\text{mix}} \rangle} \tag{48}$$

holds, where $\zeta_{A,B}$ are the friction coefficients of the pure components determined via Eq. (47). Accordingly, we have calculated

$$\frac{\rho N_L a^2}{36 \bar{M}_{\text{mon}}^2} \left(\frac{\phi_A M_A}{\eta_0^A} + \frac{\phi_B M_B}{\eta_0^B} \right) = \frac{1}{\langle \zeta^{\text{mix}} \rangle} \tag{49}$$

thereby using $\bar{M}_{\text{mon}} = 82$ g/mol and $a = 6$ Å. On the other hand, the relation

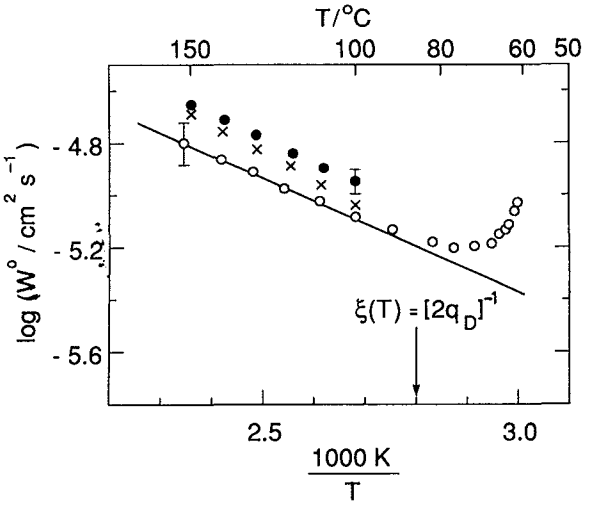

FIG. 18. An Arrhenius plot of the microscopic Rouse transition rate W^0 calculated via Eq. (40) (○). Calculation of W^0 from mechanical data assuming the fast mode approach (●) and the slow mode approach (×). A typical error bar here is determined mainly through the uncertainty in the segment length a.

$$W^0_{\text{mix}} = \frac{kT}{\langle \zeta^{\text{mix}} \rangle} \tag{50}$$

holds, hence from combining Eqs. (49) and (50), the microscopic Rouse frequency can be calculated. Equation (49) includes furthermore the so-called fast mode approach which was introduced by Kramer[61] and Sillescu.[62] These theories deal with the problem of how to connect the tracer diffusion of single species to the measured interdiffusion in a mixture. They are contrasted to theories by Brochard and de Gennes[63] and Binder[31] called the slow mode approach. There the connection between tracer diffusitivities and interdiffusion is done in a parallel addition of both parts, which means that the slower component dominates the overall dynamics. It is opposite to the ansatz we use here along Eq. (49), which means together with Eq. (48) that the constituents are added in a series leading to the domination of the faster component. At this stage, we will not discuss this point exceedingly, but will simply comment that for our particular system, because of the validity of the empirically found Eq. (48), we adopt the fast mode approach and refer for further discussion to the literature.[64] The results of our calculations are shown also in Fig. 18. The fast mode differs only in the absolute values, but the slope is identical, whereas the slow mode does not give the correct slope.

VI. CONCLUSIONS

In this paper, we have examined the critical scattering from a PDMS/PEMS blend at the critical composition by dynamic light scattering in the one phase region. The main results can be summarized as follows:

(1) the static scattering properties are well described using a mean field type of theory except;

(2) close to the critical point, a crossover to an Ising type of behavior is observed predicted by a modified Ginzburg criterion.[17,18] It gives a cross-over length of $\xi = 3.8\ R_g$, which is in fair agreement with the dynamical experimental result [cf. Fig. 15(a)]

(3) Due to the large $\xi_0 = \lim_{T \to \infty} \xi$, critical dynamics can be observed at temperatures far more apart from T_C than in any other system. That means values of $q\xi \gg 1$ can be reached relatively easy.

(4) A full understanding of the dynamical properties is only possible using mode coupled corrections originally developed by Kawasaki[36,38] and subsequently applied to polymer systems by Fredrickson.[27,28]

(5) We have for the first time analyzed properly the background and are able to verify all relevant theoretical scaling predictions (cf. Fig. 13) for the critical part of the linewidth in the hydrodynamic regime ($R_g \xi \lesssim q^{-1}$). Furthermore, we could show that the Kawasaki shape function fits the data adequately (cf. Fig. 16).

(6) Treating the background, we had to introduce a value for the Debye cutoff[37] q_D. It became apparent from our data in comparison with the work by Stepanek *et al.*[18] that q_D^{-1} is given approximately by the length $\xi = 0.1\ N^{1/2} R_g$ which governs the crossover between mode coupled to nonmode coupled dynamics being the experimental result modifying Fredrickson's work.[28] Furthermore we could show the crossover from the hydrodynamic regime to the critical nondiffusive regime, where the linewidth becomes independent of temperature. All these relevant cross-over phenomena are depicted in Fig. 15(b).

(7) We have found that the mode coupled dynamics reaches far into the mean field regime. This is theoretically[28] not yet understood, but also confirmed experimentally by Stepanek *et al.*[18]

(8) In the regime where ξ is smaller than R_g, we were able to calculate the microscopic Rouse rate W^0 from independent viscosity measurements and compared it quantitatively with the results for W^0 from scattering (cf. Fig. 18).

ACKNOWLEDGMENTS

The authors are indebted to G. H. Fredrickson, K. Kawasaki, T. Nose, J. V. Sengers, and P. Stepanek for helpful and illuminating discussions. Special thanks to M. Benmouna and D. Schwahn who have carefully read the manuscript and helped to clarify the issue. Furthermore we thank L. Giebel for doing additional measurements and calculations. We also thank R. Thomas for computational assistance. One of us (B. M.) thanks the Claussen Stiftung im Stifterverband der deutschen Industrie for a stipend.

[1] T. Hashimoto and I. Kumaki, Macromolecules **16**, 641 (1983).
[2] M. Okada and C. C. Han, J. Chem. Phys. **85**, 5317 (1986).
[3] F. S. Bates and P. Wiltzius, J. Chem. Phys. **91**, 3258 (1989).
[4] G. Ronca and T. P. Russell, Phys. Rev. B **35**, 8566 (1987).
[5] H. Meier and G. Strobl, Macromolecules **20**, 649 (1987).
[6] G. Shibayama, H. Young, R. S. Stein, and C. C. Han, Macromolecules **18**, 2179 (1983).
[7] D. Schwahn, K. Mortensen, T. Springer, H. Yee-Madeire, and R. Thomas, J. Chem. Phys. **87**, 6078 (1987).

[8] A. Lapp, C. Picot, and H. Benoit, Macromolecules **18**, 2437 (1985).
[9] J. S. Higgins and A. I. Carter; Macromolecules **17**, 2197 (1984).
[10] M. G. Brereton, E. W. Fischer, and Ch. Herkt-Maetzky, J. Chem. Phys. **87**, 6144 (1987).
[11] W. G. Jung and E. W. Fischer, Makromol. Chem. Makromol. Symp. **16**, 281 (1988).
[12] Ch. Herkt-Maetzky and J. Schelten, Phys. Rev. Lett. **51**, 96 (1983).
[13] P. G. de Gennes, *Scaling Concepts in Polymer Physics* (Cornell University, Ithaca, 1979).
[14] D. Schwahn, K. Mortensen, and Yee-Madeira, Phys. Rev. Lett. **58**, 1544 (1987).
[15] P. G. de Gennes, J. Phys. (Paris) **38**, L441 (1977).
[16] J. F. Joanny, J. Phys. A **11**, L117 (1978).
[17] F. S. Bates, I. H. Rosedale, P. Stepanek, T. P. Lodge, P. Wiltzius, G. H. Fredrickson, and R. P. Hyelm, Phys. Rev. Lett. **65**, 1839 (1990).
[18] P. Stepanek, T. P. Lodge, C. Kedrowski, and F. S. Bates, J. Chem. Phys. **94**, 8289 (1991).
[19] R. Schneider, L. Belkoura, I. Schelten, D. Woermann and B. Chu, Phys. Rev. B **22**, 5507 (1980).
[20] K. Hamano, T. Nomura, K. Kawazura, and N. Kuwahara, Phys. Rev. A **26**, 1153 (1982).
[21] M. Takahashi and T. Nose, Polymer J. **16**, 771 (1984).
[22] M. Fixmann, J. Chem. Phys. **36**, 310 (1962).
[23] L. P. Kadanoff and I. Swift, Phys. Rev. **166**, 89 (1968).
[24] K. Kawasaki, in *Phase Transitions and Critical Phenomena*, edited by C. Domp and M. S. Green (Academic, New York, 1976), Vol. 5a.
[25] B. I. Halperin, P. C. Hohenberg, and E. B. Siggia, Phys. Rev. Lett. **32**, 1289 (1974).
[26] E. B. Siggia, B. I. Halperin, and P. Hohenberg, Phys. Rev. B **13**, 2110 (1976).
[27] G. H. Fredrickson and F. S. Bates; J. Chem. Phys. **85**, 633 (1986).
[28] G. H. Fredrickson, J. Chem. Phys. **85**, 3556 (1986).
[29] M. G. Brereton, E. W. Fischer, G. Fytas, and U. Marschall, J. Chem. Phys. **86**, 5174 (1987).
[30] H. Benoit, W. Wu, M. Benmouna, B. Mozer, B. Bauer, and A. Lapp, Macromolecules **18**, 986 (1985).
[31] K. Binder, J. Chem. Phys. **79**, 6387 (1983).
[32] H. E. Stanley, *Phase Transitions and Critical Phenomena* (Clarendon, Oxford, 1971).
[33] S. Janβen, D. Schwahn, and T. Springer, Phys. Rev. Lett. **68**, 3180 (1992).
[34] H. Swinney and D. Henry, Phys. Rev. A **8**, 2586 (1973).
[35] L. van Hove, Phys. Rev. **95**, 1374 (1954).
[36] K. Kawasaki, Ann. Phys. (N.J.) **61**, 1 (1970).
[37] K. Perl and R. Ferrell, Phys. Rev. Lett. **29**, 51 (1972).
[38] K. Kawasaki and T. Ohta, Prog. Theor. Phys. **59**, 362 (1978).
[39] K. Kawasaki and S. Lo, Phys. Rev. Lett. **29**, 48 (1972).
[40] F. Brochard and P. G. de Gennes, Phys. Status Solidi A **118**, 289 (1983).
[41] K. Schweizer, J. Chem. Phys. **91**, 5802 (1989).
[42] B. Momper, Ph.D. thesis, University of Mainz, 1989.
[43] W. Thönnes, Ph.D. thesis, University of Mainz, 1990.
[44] J. P. Kratohvil, G. Dezelic, M. Kerker, and E. Matijevic, J. Polymer Sci. **57**, 59 (1962).
[45] T. M. Bender, R. J. Lewis, and R. Pecora, Macromolecules **19**, 244 (1986).
[46] C. H. Wang, G. Fytas, G. Lilge, and Th. Dorfmüller, Macromolecules **14**, 1363 (1981).
[47] R. F. Chang, H. Burstyn, and J. V. Sengers; Phys. Rev. A **19**, 866 (1979).
[48] Recent results concerning $\chi=\chi(T,\phi)$ can be found in M. G. Bawendi and K. F. Freed; J. Chem. Phys. **88**, 2741 (1988) and J. Dudowicz and K. F. Freed; Macromolecules **23**, 1519 (1990).
[49] Z. Y. Chen, P. C. Albright, and J. V. Sengers, Phys. Rev. A **41**, 3161 (1990).
[50] Z. Y. Chen, A. Abbaci, S. Tang, and J. V. Sengers, Phys. Rev. **42**, 4470 (1990).
[51] M. A. Anisimov, S. B. Kiselev, S. Tang, and J. V. Sengers, Physica A (to be published).
[52] L. Fetters (private communication).
[53] P. F. Green and B. L. Doyle, Macromolecules **20**, 2471 (1987).
[54] J. Kanetakis and G. Fytas, Macromolecules **22**, 3452 (1989).
[55] D. Oxtobx and W. Gelbart, J. Chem. Phys. **61**, 2957 (1973).
[56] Q. H. Lao, B. Chu, and N. Kuwahara, J. Chem. Phys. **62**, 2039 (1975).
[57] T. Katuoka and S. Ueda, J. Polymer Sci. Polymer Lett. Ed. **4**, 317 (1966).
[58] J. V. Sengers, Int. J. Thermophys. **6**, 203 (1985).
[59] J. D. Ferry, *Viscoelastic Properties of Polymer*, 3rd ed. (Wiley, New York, 1980), Chap. 10.
[60] B. Momper, G. Meier, and E. W. Fischer, J. Non-Cryst. Solids **131**, 624 (1991).
[61] E. J. Kramer, P. F. Green, and C. J. Palmstrom, Polymer **25**, 473 (1984).
[62] H. Sillescu, Makromol. Chem. Rapid Commun. **5**, 519 (1984).
[63] F. Brochard and P. G. de Gennes, Physica A **118**, 289 (1983).
[64] For experimental review, see Ref. 54; for further theoretical formulations, see K. W. Kehr, K. Binder, and S. M. Reulein, Phys. Rev. B **39**, 4891 (1989); W. Hess and A. Z. Akcasu, J. Phys. (France) **49**, 1261 (1988); A. Z. Akcasu and M. Tombakoglu, Macromolecules **23**, 607 (1990).